Heterogeneous Catalysis

DOI: 10.1002/anie.200603931

Water Gas Shift Reaction on Cu and Au Nanoparticles Supported on $CeO_2(111)$ and $ZnO(000\bar{1})$: Intrinsic Activity and Importance of Support Interactions**

José A. Rodriguez, Ping Liu, Jan Hrbek, Jaime Evans, and Manuel Pérez*

Currently, the primary source of hydrogen is steam reforming from hydrocarbons. The reformed fuel contains 1–10% CO.[1,2] The water gas shift reaction (WGS, $CO + H_2O \rightarrow H_2 + CO_2$) and preferential CO oxidation ($2CO + O_2 \rightarrow 2CO_2$) processes are critical in providing clean hydrogen for polymer electrolyte membrane fuel cells and other industrial applications.[1–3] Conventional WGS catalysts (e.g., Cu on zinc oxide) meet the needs of large stationary applications.[4] Improved air-tolerant, cost-effective WGS catalysts for lower-temperature processing are needed to enable mobile fuel-cell applications.[1–3,5] Recently, Au/CeO_2 and Cu/CeO_2 materials were reported to be very promising catalysts for the lower-temperature WGS reaction.[6,7] There is no generally accepted picture for the role of ceria and the metal in the WGS reaction. The existence and role of reduced metal nanoparticles versus cationic metal centers (e.g., $Au^{\delta+}$) are debated.[5–7] Very recent in situ measurements by near-edge X-ray absorption fine-structure (NEXAFS) spectroscopy show that $Cu^{\delta+}$ and $Au^{\delta+}$ species are not stable under the typical conditions of the WGS reaction.[7–9]

We investigated the WGS reaction on Cu and Au nanoparticles supported on $CeO_2(111)$ and $ZnO(000\bar{1})$ surfaces. Previous studies proved that well-defined single-crystal surfaces are very good models for examining the kinetics and mechanism of the WGS reaction on copper.[10–12] One of our objectives herein is to establish patterns of reactivity as a function of the adsorbed-metal (admetal) coverage and the oxide support. $CeO_2(111)$ and $ZnO(000\bar{1})$ are O-terminated surfaces. Both did not display any catalytic activity under the reaction conditions examined in this work ($P_{CO} = 20$ Torr, $P_{H_2O} = 10$ Torr, $T = 575$–650 K). Figure 1 compares the WGS activity of 0.5 monolayers (ML) of Au or Cu deposited on $CeO_2(111)$ and $ZnO(000\bar{1})$ with the corresponding activity of Au(111) and Cu(100). Images from scanning tunneling microscopy (STM) indicate that the admetals form three-dimensional particles with sizes in the range 2–4 nm when present on the clean oxide surfaces at around 600 K.[9,13] The WGS activity seen here for Cu(100) is comparable to that detected for Cu(111) or Cu(110);[10,11] variations in observed reactivity are probably a result of changes in the structure of the copper surfaces.[11] The deposition of Cu nanoparticles on $ZnO(000\bar{1})$ produces a catalyst that is clearly more active than the pure extended Cu surfaces. An even better catalyst is obtained when the nanoparticles are supported on CeO_2-(111).

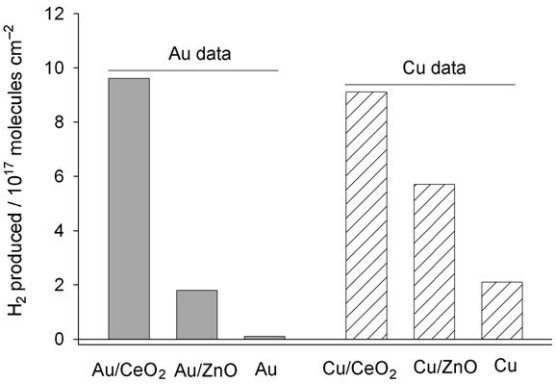

Figure 1. Amounts of H_2 produced during the WGS reaction on 0.5 ML of gold or copper deposited on $CeO_2(111)$ and $ZnO(000\bar{1})$. For comparison, the activities of Au(111) and Cu(100) are also included. The catalysts were exposed to a mixture of 20 Torr CO and 10 Torr H_2O at 625 K for 5 minutes in a batch reactor. A reaction time of 2–3 minutes was enough to reach a steady-state regime in the reactor.

We found negligible activity for the WGS reaction on Au(111) or polycrystalline Au. The $Au/ZnO(000\bar{1})$ system displayed catalytic activity that was worse than that of $Cu/ZnO(000\bar{1})$. In contrast, $Au/CeO_2(111)$ was an excellent catalyst with activity similar to that of $Cu/CeO_2(111)$. The dramatic effects of ceria on the WGS activity of Au nanoparticles are shown in Figure 2, which plots the catalytic activity as a function of Au and Cu coverage. Independently of the admetal coverage, $Au/CeO_2(111)$ is always a much better catalyst than $Au/ZnO(000\bar{1})$ or pure metallic gold.

In Figure 2, the catalytic activity of the metal/oxide systems initially increases as Au and Cu are added and reaches a maximum at around 0.4 ML for Au and around 0.5 ML for Cu. The overall catalytic activity decreases above these coverages. A similar trend was observed for the catalytic oxidation of CO on $Au/TiO_2(110)$ and attributed to a reduction in activity as a result of increasing the Au particle size.[14] STM images show that the particle size of Cu and Au on $CeO_2(111)$ or $ZnO(000\bar{1})$ rises above 4 nm and continu-

[*] Dr. J. A. Rodriguez, Dr. P. Liu, Dr. J. Hrbek
Chemistry Department
Brookhaven National Laboratory
Upton, NY 11973 (USA)
Fax: (+1) 631-344-5815
E-mail: rodrigez@bnl.gov
Dr. J. Evans, Prof. M. Pérez
Facultad de Ciencias
Universidad Central de Venezuela
Caracas 1020 A (Venezuela)

[**] This work was supported by the US Department of Energy, Office of Basic Energy Sciences, under contract DE-AC02-98CH10886.

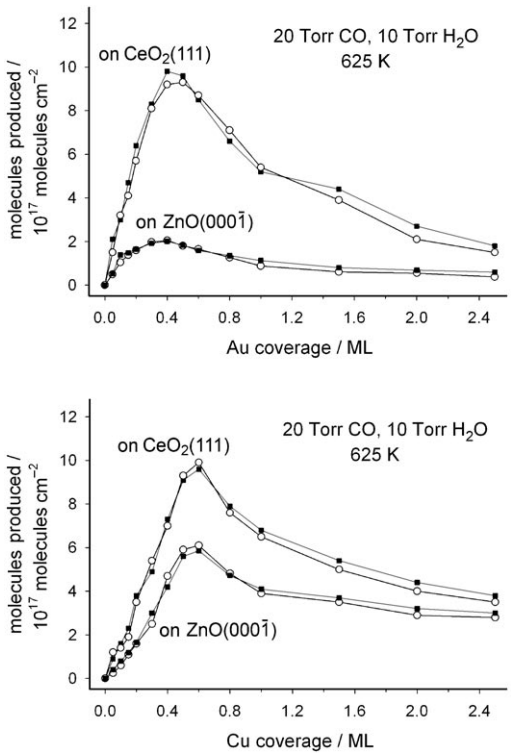

Figure 2. Top: Amounts of H_2 (■) and CO_2 (○) produced during the WGS reaction on Au/CeO_2(111) and Au/ZnO(000$\bar{1}$) catalysts. Bottom: Corresponding results for Cu/CeO_2(111) and Cu/ZnO(000$\bar{1}$) catalysts. Each surface was exposed to a mixture of 20 Torr CO and 10 Torr H_2O at 625 K for a period of 5 minutes in a batch reactor. A reaction time of 2–3 minutes was enough to reach a steady-state regime in the reactor.

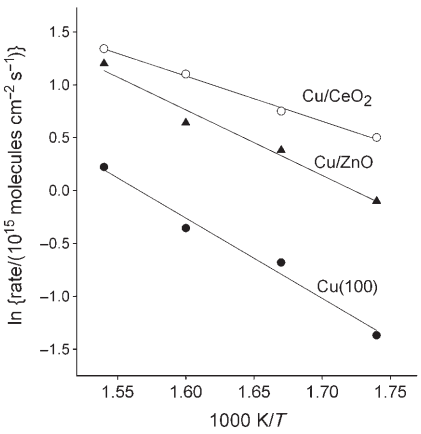

Figure 3. Arrhenius plot of the WGS reaction rate for Cu(100), 0.5 ML Cu on ZnO(000$\bar{1}$), and 0.5 ML Cu on CeO_2(111). The data were acquired with a pressure of 20 Torr CO and 10 Torr H_2O.

ously grows when the admetal coverage is increased beyond 0.5 ML.[9,13] Although the optimum WGS activity in Figure 2 is for admetal coverages of 0.4–0.5 ML, ceria-based catalysts with admetal coverages near 1 ML are still substantially better than Cu(100) or Au(111).

Experiments similar to those in Figure 1 were also done at temperatures of 575, 600, and 650 K. Again Au/CeO_2 and Cu/CeO_2 displayed superior performance. We constructed Arrhenius plots for the different surfaces by taking the natural logarithms of the reaction rates (Figure 3). On Cu(100) the apparent activation energy given by the slope of the Arrhenius plot is 15.2 kcal mol^{-1}, which is somewhat smaller than the value of 17 kcal mol^{-1} reported for the WGS reaction on a Cu(111) surface.[11] The apparent activation energy decreases to 12.4 kcal mol^{-1} on Cu/ZnO(000$\bar{1}$) and 8.6 kcal mol^{-1} on Cu/CeO_2(111). As discussed below, this decrease may be a consequence of more efficient cleavage of the O–H bonds in water. Arrhenius plots for the Au catalysts yielded apparent activation energies of 16.1 kcal mol^{-1} on Au/ZnO(000$\bar{1}$) and 7.9 kcal mol^{-1} on Au/CeO_2(111). This sequence corroborates the benefits of using ceria as a support.

The kinetic data in Figures 1, 2, and 3 were collected by using a reaction cell attached to an ultrahigh-vacuum chamber for surface characterization. The gases were pumped out of the reaction cell and the surfaces were subsequently characterized by X-ray photoelectron spectroscopy (XPS). The XPS data point to a lack of oxidation of the metals, a reduction of the ceria support, and suggest different reaction intermediates for Cu(100) and the metal/oxide catalysts. The lack of oxidation of the Cu and Au nanoparticles after the WGS reaction is consistent with in situ measurements of NEXAFS for high-surface-area catalysts,[7–9] which show that $Cu^{\delta+}$ and $Au^{\delta+}$ species are not stable under typical WGS conditions. All these studies indicate that pure Au nanoparticles form part of the active phase of the Au/CeO_2 and Au/ZnO catalysts, in contrast to an earlier hypothesis that suggested the presence of Au_2O or Au_2O_3,[6] but in agreement with the behavior of Au nanoparticles in other catalytic processes.[14–20] In the case of Cu(100), analysis of the surface after the WGS reaction showed it to be essentially free of formate and carbonate species. The same result was reported for the WGS reaction on Cu(111) and Cu(110) substrates.[11] On these extended copper surfaces, the reaction probably proceeds through a redox mechanism.[11,21,22] In contrast, XPS characterization of the metal/oxide surfaces after the WGS reaction gave the typical peaks for adsorbed formate- or carbonate-like species in the C 1s region. This result opens the possibility for a different reaction mechanism,[5,23] although the formate- or carbonate-like species could be simply spectators bound to the oxide.

Ce 3d core-level XPS spectra showed partial reduction of the ceria support after exposing Cu/CeO_2(111) and Au/Ce(111) to the WGS reaction mixture or CO. This reduction was not seen when pure CeO_2(111) was exposed to the gases. Thus, it appears that the admetals favor the formation of O vacancies in ceria. These oxygen vacancies enhance the chemical reactivity of Au nanoparticles[24,25] and could have a similar effect on Cu nanoparticles. Surface characterization of Au/ZnO(000$\bar{1}$) and Cu/ZnO(000$\bar{1}$) after the WGS reaction did not find a measurable number of O vacancies in the zinc oxide support. Such an absence of O vacancies could explain the substantial difference between the catalytic activity of the systems containing zinc oxide and systems containing ceria. Thus, the reducibility of ceria makes it a better support.

A very important issue is to establish the intrinsic reactivity of the Cu and Au nanoparticles. Can nanoparticles

of Cu and Au catalyze the WGS reaction on their own without the aid of an oxide support? Are these nanoparticles more reactive than extended surfaces of the pure metals? Theoretical studies have shown that unsupported Au nanoparticles can be very active for the oxidation of CO.[26] By using density functional calculations[27,28] we investigated the WGS reaction on Cu_{29} and Au_{29} clusters and on Cu(100) and Au(100) surfaces. The Cu_{29} and Au_{29} clusters exhibited pyramidal structures formed by the interconnection of (111) and (100) faces of the bulk metals (Figure 4). They had three layers

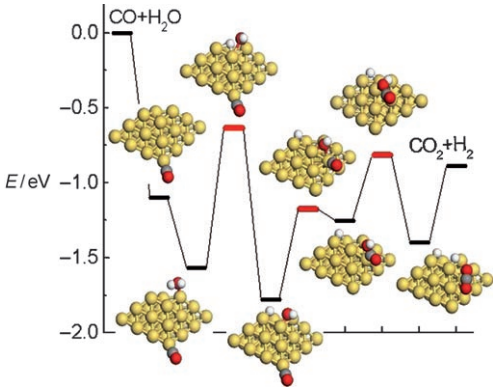

Figure 4. Reaction profile and structures for the WGS reaction on a Cu_{29} nanoparticle. The zero energy is taken as the sum of the energies of the bare nanoparticle, gas-phase water, and carbon monoxide. The red bars represent the transition states, and the black bars represent reactants, intermediates, or products. Cluster side view: yellow Cu, red O, gray C, white H.

containing 16, 9, and 4 metal atoms.[29] Similar Cu and Au clusters have been observed on $CeO_2(111)$ by STM.[13] Thus, Cu_{29} and Au_{29} can be taken as reasonable models for the nanoparticles.

Figure 4 shows the calculated energy changes for the WGS reaction on a Cu_{29} cluster. The reaction pathway with the minimum energy barriers involves the following steps [Eqs. (1)–(6)]:

$$CO_{(g)} \rightleftharpoons CO_{(ads)} \quad (1)$$

$$H_2O_{(g)} \rightleftharpoons H_2O_{(ads)} \quad (2)$$

$$H_2O_{(ads)} \rightarrow OH_{(ads)} + H_{(ads)} \quad (3)$$

$$CO_{(ads)} + OH_{(ads)} \rightarrow OCOH_{(ads)} \quad (4)$$

$$OCOH_{(ads)} \rightarrow CO_{2\,(g)} + H_{(ads)} \quad (5)$$

$$2\,H_{(ads)} \rightarrow H_{2\,(g)} \quad (6)$$

The adsorption of CO or H_2O on the Cu particle is clearly exothermic. The first and most important energy barrier is for the dissociation of water into adsorbed OH and H. Then, the reaction of OH and CO produces an OCOH species. The final important energy barrier is for the decomposition of the OCOH intermediate into CO_2 gas and adsorbed H, which eventually yields H_2 gas. The DFT results indicate that a free Cu particle can catalyze the WGS reaction easily. A comparison with the corresponding results on Cu(100) shows that the dissociation of water on the extended surface has a larger activation barrier (1.13 eV vs. 0.94 eV on the nanoparticle) and that no stable OCOH intermediate is formed, as a redox mechanism operates.[21] The presence of corner or edge atoms in Cu_{29} favors the dissociation of H_2O, which is consistent with the relatively faster rate previously reported for Cu(110) relative to Cu(111).[11]

The DFT results for the WGS reaction on Au_{29} or Au(100) indicate that these systems cannot catalyze the reaction. Neither surface is able to adsorb or dissociate water molecules. Figure 5 shows a correlation between the calcu-

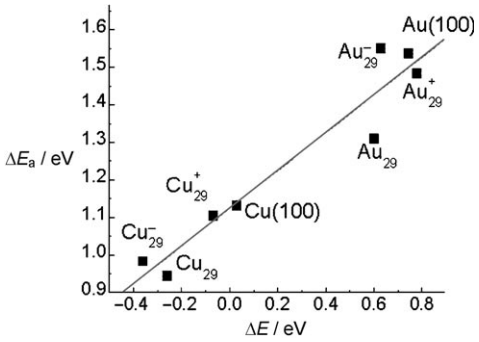

Figure 5. Correlation between the calculated barrier (ΔE_a) and the calculated reaction energy (ΔE) for water dissociation on several copper and gold systems.

lated barrier (y axis) and the calculated reaction energy (x axis) for water dissociation on Au(100), Cu(100), as well as ionic and neutral Au_{29} and Cu_{29} nanoparticles. All the gold systems are characterized by a large activation barrier and an endothermic ΔE value. There is a significant improvement in chemical reactivity in going from Au(100) to Au_{29},[29] but not enough for dissociation of the water molecule. The addition of charge to the Au nanoparticle to form either Au_{29}^- or Au_{29}^+ also does not help. These results cannot explain the large catalytic activity seen for $Au/CeO_2(111)$ (Figure 2) and highlight the important role of ceria in the activation of the system. Unfortunately, we could not perform density functional calculations for $Au/CeO_2(111)$ surfaces. Because of the incorrect description of the highly localized 4f states in Ce ions, DFT cannot be used to treat the electronic structure of ceria surfaces that contain O vacancies or other structural defects.[30,31] The Hubbard U correction mitigates this problem,[30–32] but has not been tested in studies dealing with the energetics of surface reactions.

A perfect $CeO_2(111)$ surface does not dissociate water at low or high temperatures. In contrast, when O vacancies are present, the H_2O molecule dissociates on the ceria surface. Our experimental results show that Cu and Au nanoparticles promote the partial reduction of $CeO_2(111)$ by CO or the CO/H_2O mixtures typically used in the WGS reaction. Thus, in an indirect way the admetals facilitate the most difficult step in the water gas shift reaction: the dissociation of H_2O. The behavior of Au/ceria in the WGS reaction illustrates the

importance of cooperative effects for the activity of supported Au nanocatalysts.

Experimental Section

The experiments were performed in an ultrahigh-vacuum (UHV) chamber with an attached high-pressure cell or batch reactor.[9,11] The sample could be transferred between the reactor and vacuum chamber without exposure to air. The UHV chamber (base pressure ca. 1×10^{-10} Torr) was equipped with instrumentation for XPS, low-energy electron diffraction, and thermal-desorption mass spectroscopy (TDS). The Cu(100), Au(111), ZnO(000$\bar{1}$), and CeO_2(111) surfaces were cleaned by following standard procedures.[9,11,24,29] Cu and Au were vapor-deposited onto ZnO(000$\bar{1}$) or CeO_2(111) at room temperature;[9,24,33] the sample was then heated to the WGS reaction temperature. The flux of the metal was calibrated by depositing Cu or Au onto a Mo(100) crystal and measuring the TDS spectra of the admetals.[24,34] For the kinetic measurements, the sample was transferred to the batch reactor at around 300 K, the reactant gases were introduced (20 Torr CO, and 10 Torr H_2O), and then the sample was rapidly heated to the reaction temperature (575, 600, 625, or 650 K). Product yields were analyzed by a gas chromatograph.[11] The amount of molecules produced was normalized by the active area exposed by the sample. The sample holder was passivated by extensive sulfur poisoning (exposure to H_2S) and has no catalytic activity. In our reactor, a steady-state regime for the production of H_2 and CO_2 was reached after 2–3 minutes. The kinetic experiments were performed in the limit of low conversion ($< 5\%$).

The unrestricted density functional calculations were performed by using the DMol^3 code with effective core potentials, a numerical basis set, and the GGA-PW91 description of the exchange and correlation functionals.[28] Transition states were identified by using a combination of synchronous transit methods and eigenvector following, and verified by the presence of a single imaginary frequency from a sequential vibrational frequency analysis. Cu(100) and Au(111) were modeled by four-layer slabs.[35] During the density functional calculations, the geometries of the top two layers of the slabs and the Cu_{29} and Au_{29} clusters were fully relaxed.

Received: September 25, 2006
Published online: January 5, 2007

Keywords: copper · density functional calculations · gold · heterogeneous catalysis · water gas shift reaction

[1] Y. Liu, Q. Fu, M. Flytzani-Stephanopoulos, *Catal. Today* **2004**, *93–95*, 241.
[2] D. J. Suh, C. Kwak, J. H. Kim, S. M. Kwon, T. J. Park, *J. Power Sources* **2005**, *142*, 70.
[3] C. Song, *Catal. Today* **2002**, *77*, 17.
[4] D. S. Newsome, *Catal. Rev. Sci. Eng.* **1980**, *21*, 275.
[5] R. Burch, *Phys. Chem. Chem. Phys.* **2006**, *8*, 5483.
[6] Q. Fu, H. Saltsburg, M. Flytzani-Stephanopoulos, *Science* **2003**, *301*, 935.
[7] X. Wang, J. A. Rodriguez, J. C. Hanson, D. Gamarra, A. Martínez-Arias, M. Fernández-García, *J. Phys. Chem. B* **2006**, *110*, 428.
[8] D. Tibiletti, A. Amieiro-Fonseca, R. Burch, Y. Chen, J. M. Fisher, A. Coguet, C. Hardacre, P. Hu, D. Thompsett, *J. Phys. Chem. B* **2005**, *109*, 22553.
[9] X. Wang, J. A. Rodriguez, J. C. Hanson, M. Pérez, J. Evans, *J. Chem. Phys.* **2005**, *123*, 221101.
[10] C. T. Campbell, K. A. Daube, *J. Catal.* **1987**, *104*, 109.
[11] J. Nakamura, J. M. Campbell, C. T. Campbell, *J. Chem. Soc. Faraday Trans.* **1990**, *86*, 2725.
[12] C. V. Ovesen, P. Stoltze, J. K. Nørkskov, C. T. Campbell, *J. Catal.* **1992**, *134*, 445.
[13] S. Oyama, T. Ito, J. A. Rodriguez, J. Nakamura, unpublished results.
[14] M. Walden, X. Lai, D. W. Goodman, *Science* **1998**, *281*, 1647.
[15] M. Haruta, *Catal. Today* **1997**, *36*, 153.
[16] J. A. Rodriguez, *Dekker Encyclopedia of Nanoscience and Technology*, Marcel Dekker, New York, **2004**, pp. 1297–1304.
[17] M. S. Chen, D. W. Goodman, *Science* **2004**, *306*, 252.
[18] C. T. Campbell, *Science* **2004**, *306*, 234.
[19] I. N. Remediakis, N. Lopez, J. K. Nørskov, *Angew. Chem.* **2005**, *117*, 1858; *Angew. Chem. Int. Ed.* **2005**, *44*, 1824.
[20] H. Häkkinen, S. Abbet, A. Sanchez, U. Heiz, U. Landman, *Angew. Chem.* **2003**, *115*, 1335; *Angew. Chem. Int. Ed.* **2003**, *42*, 1297.
[21] N. Schumacher, A. Boisen, S. Dahl, A. A. Gokhale, S. Kandoi, L. C. Grabow, J. A. Dumesic, M. Mavrikakis, I. Chorkendorff, *J. Catal.* **2005**, *229*, 265.
[22] T. Bunluesin, R. J. Gorte, G. W. Graham, *Appl. Catal. B* **1998**, *15*, 107.
[23] S. Ricote, G. Jacobs, M. Milling, Y. Ji, P. M. Patterson, B. H. Davis, *Appl. Catal.* **2006**, *303*, 35.
[24] J. A. Rodriguez, M. Pérez, J. Evans, G. Liu, J. Hrbek, *J. Chem. Phys.* **2005**, *122*, 241101.
[25] A. Abad, P. Concepción, A. Corma, H. García, *Angew. Chem.* **2005**, *117*, 4134; *Angew. Chem. Int. Ed.* **2005**, *44*, 4066.
[26] N. Lopez, J. K. Nørskov, *J. Am. Chem. Soc.* ***2002***, *124*, 11262.
[27] P. Liu, J. A. Rodriguez, *J. Am. Chem. Soc.* **2005**, *127*, 14871.
[28] P. Liu, J. A. Rodriguez, *J. Phys. Chem. B* **2006**, *110*, 19418.
[29] L. Barrio, P. Liu, J. A. Rodriguez, J. M. Campos-Martin, J. L. G. Fierro, *J. Chem. Phys.* **2006**, *125*, 164715.
[30] M. Nolan, S. C. Parker, G. W. Watson, *Surf. Sci.* **2005**, *595*, 223.
[31] M. Nolan, S. C. Parker, G. W. Watson, *J. Phys. Chem. B* **2006**, *110*, 2256.
[32] H. J. Kulik, M. Cococcioni, D. A. Scherlis, N. Marzari, *Phys. Rev. Lett.* **2006**, *97*, 103001.
[33] X. Zhao, J. Hrbek, J. A. Rodriguez, M. Pérez, *Surf. Sci.* **2006**, *600*, 229.
[34] J. A. Rodriguez, T. Jirsak, S. Chaturvedi, *J. Chem. Phys.* **1999**, *111*, 8077.
[35] P. Liu, J. A. Rodriguez, J. T. Muckerman, J. Hrbek, *Phys. Rev. B* **2003**, *67*, 155416.

